ARTICLE

Organic–Organic Heteroepitaxy of Red-, Green-, and Blue-Emitting Nanofibers

Clemens Simbrunner,[†,*] Francesco Quochi,[‡] Gerardo Hernandez-Sosa,[†] Martin Oehzelt,[§] Roland Resel,[⊥] Günter Hesser,[∥] Martin Arndt,[∥] Michele Saba,[‡] Andrea Mura,[‡] Giovanni Bongiovanni,[‡] and Helmut Sitter[†]

[†]Institute of Semiconductor and Solid State Physics, Johannes Kepler University Linz, Austria, [‡]Dipartimento di Fisica, Università di Cagliari, SLACS-INFM/CNR, I-09042 Monserrato (CA), Italy, [§]Institute of Experimental Physics, Johannes Kepler University Linz, Austria, [⊥]Institute of Solid State Physics, Graz University of Technology, Austria, and [∥]ZONA (Zentrum f. Oberflächenund Nanoanalytik), Johannes Kepler University Linz, Austria

ABSTRACT Self-assembly processes and organic–organic heteroepitaxy are powerful techniques to obtain highly ordered molecular aggregates. Here we demonstrate that combining both methods allows not only to fabricate highly crystalline and uniaxially oriented self-assembled nanofibers but also to tune their polarized emission. We show that submonolayer coverage of sexithiophene on top of para-sexiphenyl nanofibers is sufficient to change their emission color from blue to green. Triband emission in the red, green, and blue is generated in nanofibers with thicker sexithiophene coverage, where layers of co-oriented crystals are separated by green-emitting molecular sheets.

KEYWORDS: organic–organic heteroepitaxy · para-hexaphenyl · sexithiophene · organic fluorescent nanofibers · organic–organic multilayer structures

In recent years, heteroepitaxy of organic–organic nanostructures has been demonstrated as a valuable technique to explore the full potential of organic semiconductors for optoelectronic applications. Crystalline and highly ordered heterostructures with different morphology and molecular orientations can be realized by heteroepitaxy starting from conjugated oligomers, aimed at tailoring their optical properties and transport characteristics.[1−5] Para-hexaphenyl (p-6P) and α-sexithiophene (6T) are good model systems for heteroepitaxy as well as important oligomers for device applications, and hence, several studies have been conducted on the p-6P/6T material couple. It has been shown that both p-6P and 6T crystalline thin films can be used as organic templates to obtain highly crystalline organic–organic heterostructures in which p-6P and 6T molecules are both standing or parallel to the substrate.[3,4]

Here we propose a new p-6P/6T heteroepitaxy scheme on muscovite mica, a sheet silicate, yielding highly crystalline and oriented nanofibers. New optical functionalities are enabled which originate at the submonolayer scale and cannot be deduced from the results of structural and morphological characterization. Highly crystalline and oriented p-6P nanofibers on muscovite have already been realized (see Figure 1a),[6−8] showing, for example, optical polarization anisotropy,[9] guidance,[10] and amplification of the material deep-blue spontaneous emission,[11] parametric upconversion of near-infrared light,[12] and laser action on random optical modes established along the fibers' axes.[11] On the contrary, orange-red-emitting crystalline 6T nanofibers on muscovite grow along multiple azimuthal orientations (Figure 1a)[13] and therefore strongly hamper the macroscopic polarization state of the emitted light.

In this study, we show that p-6P nanofibers on muscovite can be used as templates for the self-assembly of oriented p-6P/6T heterostructure nanofibers. We demonstrate by photoluminescence spectroscopy that emission chromaticity of p-6P/6T nanofibers is a function that can be tuned by varying the 6T deposition time. In the submonolayer limit, the 6T heterolayer is emitting in the green spectral range and its emission spectrum is similar to that of a solvated 6T phase. For longer deposition time, crystal nucleation occurs and a red-orange emission overlaps the green one. The strong polarization anisotropy of p-6P nanofibers is preserved by the parallel alignment of 6T molecules, forced by the epitaxial relationship between p-6P and 6T at the interfacial layer. Combined X-ray diffractometry (XRD), atomic force microscopy (AFM), transmission electron microscopy (TEM), and scanning Auger microscopy (SAM) complements optical spectroscopy technique and provides a clear picture of heterolayer crystal structure, composition, and morphology.

*Address correspondence to clemens.simbrunner@jku.at.

Received for review August 3, 2010 and accepted September 22, 2010.

Published online September 29, 2010. 10.1021/nn1018889

RESULTS AND DISCUSSION

Immediately after cleaving, the muscovite mica substrates are transferred *via* a load lock to the growth chamber that is equipped with a hot wall epitaxy (HWE) reactor[14,15] for p-6P and a separate one for 6T evaporation. During the whole deposition procedure, samples are continuously heated to 120 °C, ensuring stable growth conditions. In a first step, a p-6P template (sketched in Figure 1a) is grown with a nominal layer thickness of 120 nm. In a further growth stage, the samples are automatically transferred in high vacuum conditions to the 6T source oven. In order to investigate sample properties in correlation with 6T deposition time, a complete series of samples has been fabricated and analyzed. In particular, samples with a nominal 6T coverage of less than 1 nm (representative for the situation sketched in the left panel of Figure 1b) up to half a micrometer (compare right panel of Figure 1b) have been investigated.

The optical response of p-6P/6T heteroepitaxial films is investigated by epifluorescence microscopy under UV photoexcitation by a lamp or scanning laser (Figure 1b (right),c). Fluorescence images reveal that p-6P/6T heteroepitaxy on muscovite mica leads to the formation of highly oriented fibers as in the case of pure p-6P (left panel, Figure 1a). With 6T submonolayer coverages, green-emitting fibers are obtained. The emission spectrum is dominated by that of the 6T molecules deposited on top of the p-6P fibers (green dashed line in Figure 2a), while no fluorescence is detected between adjacent fibers. From the observed p-6P emission quenching and the results of transient photoluminescence experiments (not reported in this work), we infer that the emission of the 6T submonolayer is sensitized by the excited p-6P crystalline material of the fibers *via* energy transfer.

For increasing 6T coverage thickness, the red-orange fluorescence band typical of 6T polycrystalline films appears (the spectrum is plotted as a red dashed line in Figure 2a), suggesting that crystal nucleation occurs on top of the fibers. The emission intensity of the new band is much weaker than that of a submonolayer film grown on p-6P fibers, whereas it is comparable to that of a pure 6T/muscovite film of polyoriented crystalline fibers (right panel, Figure 1a) grown with similar deposition time.

Scanning probe fluorescence images collected in different spectral bands make it possible to map the distributions of green-emitting 6T molecules and 6T crystals along the 6P template fibers. Fluorescence intensity measured through a green band-pass filter (right panel, Figure 1c) shows quite a homogeneous distribution of green-emitting molecules, whereas fluorescence imaging through a red-transmitting filter proves that 6T crystals are superimposed to the templating fibers and form fibers themselves (left panel, Figure 1c). Red emission spatially overlaps the green one, and the emission

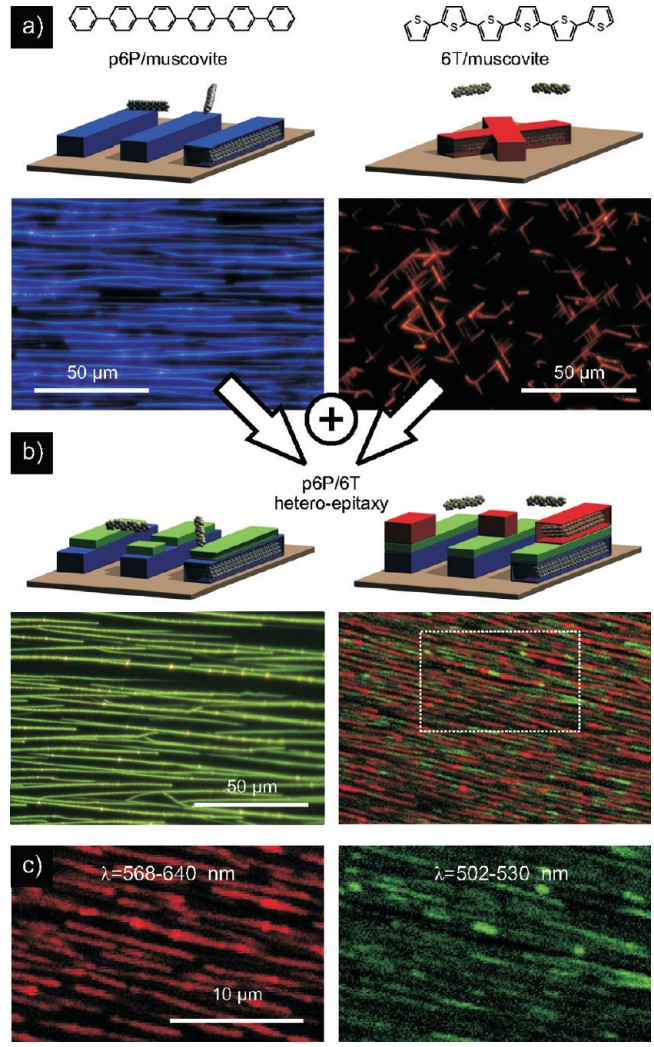

Figure 1. (a) Deep-blue-emitting highly oriented p-6P nanofibers (left) and red-orange 6T fibers (right) grown on muscovite mica. (b) p-6P/6T fibers obtained with nominally submonolayer coverage of 6T (left) and p-6P template fibers overgrown with nominally 400 nm 6T (right). Schematic representations of multilayer fibers are provided above, with crystalline p-6P represented by blue sticks, interfacial 6T submonolayer as the green sheets, and crystalline 6T as red sticks. (c) Epifluorescence images acquired through green and red band-pass filters are shown as magnification of the white boxed region in the right part of section (b).

spectrum can be quite well reproduced by a superposition of 6T submonolayer and crystal spectra. Thus, green-emitting 6T molecules are suggested to persist as an interfacial submonolayer at the p-6P/6T crystal boundaries. It is noteworthy that the spectrum of the 6T submonolayer film (Figure 2a) is considerably blue-shifted with respect to that of 6T crystals and only slightly red-shifted from that of monomers in solution.[16] This is reminiscent of what has been reported for submonolayer films of laying 6T molecules deposited on silicon dioxide, which was explained as an effect due to intermolecular coupling caused by J-type aggregation.[17] Besides the role played by 6T−6T intermolecular interactions in submonolayer films, a wavelength shift in emission could also stem from dielectric

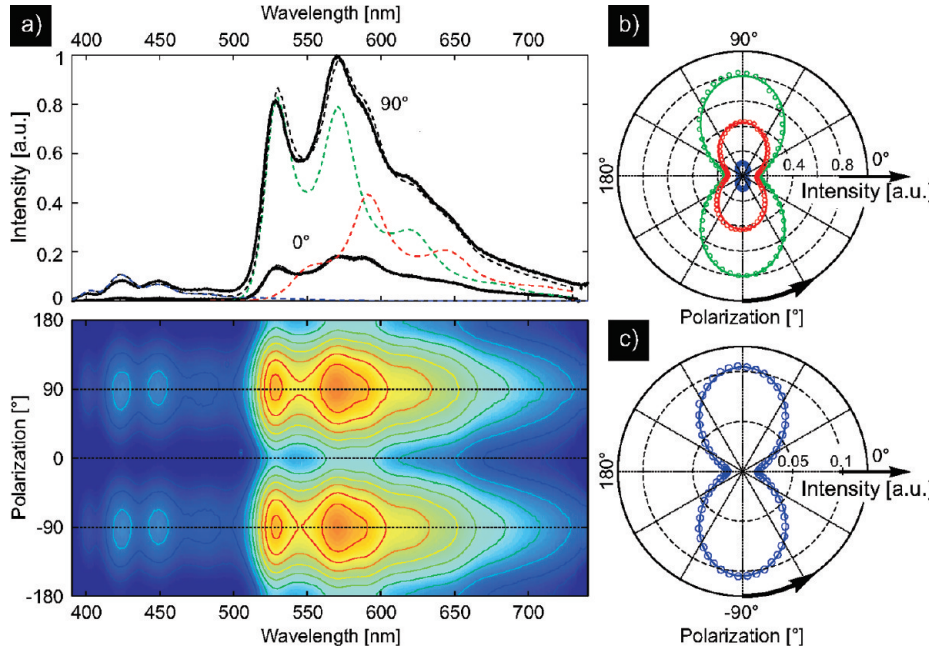

Figure 2. (a) Top panel: fluorescence spectra of a film with nominally 400 nm 6T fiber thickness, acquired at 0° (long fiber axis) and 90° polarization angle. The blue, green, and red dashed lines represent the fitted contribution of blue (p-6P), green (interfacial 6T submonolayer), and red (crystalline 6T) components. Bottom panel: false-color-coded polarization wavelength spectrogram of the fluorescence intensity. Isointensity lines are also displayed. (b) Polar plot of the p-6P and 6T material phases' fluorescence intensity *versus* polarization angle. (c) Contribution of crystalline p-6P to the single spectra, representing a magnification of section (b) for better visibility (solid lines represent a $\cos^2$ fit to the experimental data).

effects relating to the materials underlying 6T molecules.

Optical anisotropy, molecular orientation, and long-range order of the p-6P/6T heteroepitaxial films are investigated by combined fluorescence spectroscopy and fluorescence polarization analysis averaged over sample areas as large as 500 μm^2. The emission spectrum of the films can be decomposed in its three components arising from crystalline p-6P, interfacial 6T submonolayers, and crystalline 6T, which emit in the blue, green, and red, respectively. The three components are singled out from the emission spectrum by measuring pure p-6P films, p-6P/6T films with 6T submonolayer coverage, and pure 6T films on muscovite mica (dashed lines in Figure 2a). A linear superposition of the three reference spectra fits well to the emission spectrum, hinting to the potential ability of tuning the chromaticity of the 6T/p-6P fibers across the entire visible spectrum by changing layer thickness. Polarization-resolved measurements can then be used to determine molecular orientation of each material phase within the fibers. The polar plot of fitted spectral weights *versus* polarization angle is shown in Figure 2b. Strong polarization anisotropy is demonstrated by the high (up to 9 dB) ratios obtained between fluorescence intensity maxima and minima *versus* angle. Fluorescence anisotropy shows that emission dipoles and thereby the long molecular axis, of crystalline p-6P, interfacial 6T, and crystalline 6T are fairly well-aligned along the same direction, that is, perpendicular to the fibers' axis (at 0° angle). Fluorescence excitation experiments with variable polarization angle of the laser pump show that optical absorption is also polarized (see Supporting Information), thereby confirming the orientational order of molecules in different p-6P and 6T phases deduced from polarization analysis of the fluorescence. Overall, fluorescence microscopy and spectroscopy demonstrate the ability of organic epitaxy to drive the growth of highly oriented 6T fibers on p-6P fiber templates. The p-6P/6T interface exhibits the presence of co-oriented molecules that are determinant for the fiber emission color. Structural and morphological studies are necessary to determine the epitaxial relationships between material crystal phases as well as fibers' topography.

In a further step, the crystallographic structure of a 120 nm/400 nm thick p-6P/6T organic−organic heterostructure has been analyzed by $\Theta/2\Theta$ specular scans, presented in Figure 3a. The specular scan shows clearly three diffraction peaks (located at 1.258, 1.378, and 1.422 $Å^{-1}$), which can be attributed to muscovite mica (004), the β-phase of p-6P ($11\bar{1}$),[18] and the so-called low-temperature phase of 6T ($\bar{4}11$),[19] respectively. This means that 6T ($\bar{4}11$) netplanes are aligned parallel to the substrate surface and that the long molecular axes (LMA) of 6T are nearly parallel to the substrate. For p-6P, the same holds true. The (004) peak of muscovite mica obviously originates from the (001) oriented substrate. In order to deduce the epitaxial relationships between both organic crystals and in further consequence the azimuthal molecular alignment, XRD pole figure mea-

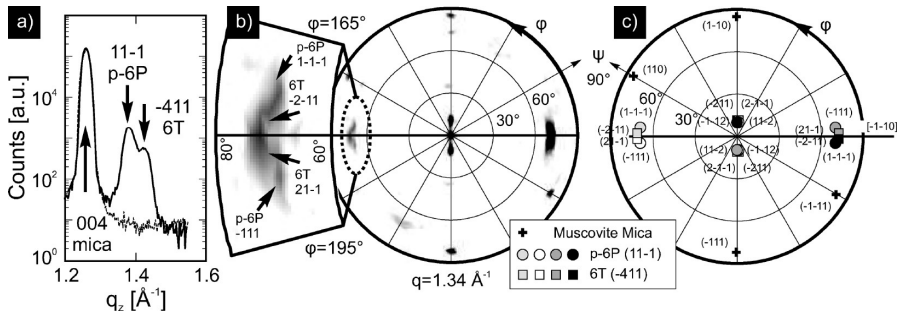

Figure 3. (a) Specular XRD scan of organic heterostructure showing muscovite mica (004), p-6P (11$\bar{1}$), and 6T ($\bar{4}$11) reflections. In comparison, the dashed line presents an analogue scan on pure mica. (b) XRD pole figure measurement (q = 1.34 Å^{-1}) providing information about the azimuthal orientation of the p-6P and 6T crystals relative to the muscovite mica substrate. The inset provides a zoom of the pole figure, indicating the presence of p-6P and 6T crystallites. (c) Stereogram of the presented pole figure measurement.

surements have been performed. In particular, the azimuthal orientation of ($\bar{2}$11) of 6T (q = 1.34 Å^{-1}) has been analyzed in detail and is reported in Figure 3b. Experiments reveal two significant spots located symmetrically aligned around the [110] direction of muscovite mica and are consequently characteristic for a single fiber domain deposited on an α cleavage plane.[20] A more detailed analysis of the pole figure (see the inset in Figure 3b) allows one to resolve additional distinct diffraction peaks originating from the {21$\bar{1}$} netplanes of 6T as well as from the {$\bar{1}$11} netplanes of p-6P. A complete analysis of the pole figure measurement is demonstrated in Figure 3c, describing the observed diffraction patterns by four crystallites of each molecular species representing a two-fold symmetry with an additional mirror axis around the [110] direction of muscovite mica.[21]

On the basis of the pole figure analysis, a real space model of the crystal and molecular orientations is given in Figure 4a. The crystal stack on the left side demonstrates the molecular orientation of p-6P (gray) molecules in one crystallite, and the white arrow points in the [1$\bar{1}$0] direction of the p-6P stack, defining the resulting long fiber axis (LFA).[20] On top of the organic template, 6T molecules (yellow atoms represent sulfur) are indicated, packed in the low-temperature herringbone structure and characterized by a ($\bar{4}$11) contact plane parallel to the substrate surface. A more detailed inspection of the p-6P/6T interface (shown in the inset of Figure 4a) resolves the expected herringbone package providing nearly perfect adoption of 6T to p-6P layers. To aide the reader, the mirrored crystallite is reduced to two single molecules and the corresponding LFA that has an angle of 6° with respect to the [110] direction of muscovite mica. As a consequence of these orientations, both long molecular axes (LMA) are parallel to each other and have an angle of 83° with respect to the high symmetry axis of muscovite mica. A splitting of the LFA around the [110] direction of muscovite mica due to mirror symmetry can be further outlined by the morphological arrangement of two single nanofibers seen in the center of the plot (Figure 4a).

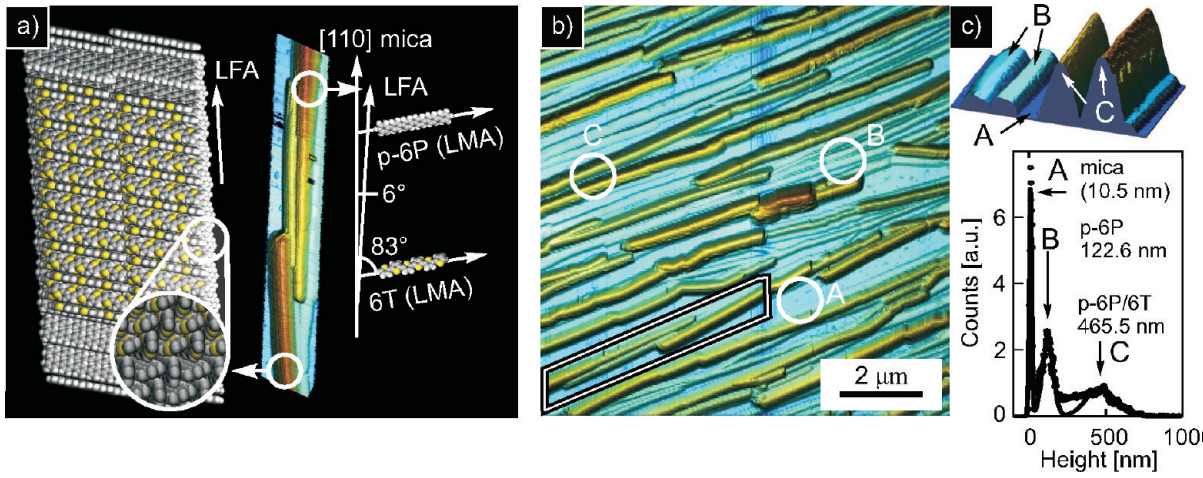

Figure 4. (a) Simulation of the molecular alignment within the nanofibers concluded from the XRD measurements. The angle between the long fiber axis (LFA), the long molecular axis (LMA), and the mica [110] direction is indicated in the mirrored crystal model on the right. The inset indicates the herringbone structure of p-6P and 6T at the crystal interface. (b) AFM image of the heteroepitaxial sample structure showing parallel aligned nanofibers. The polygon indicates the region depicted in panel (a). (c) Height histogram of AFM image showing three peaks originating from the bare mica substrate, visible between the fiber structures (A), the p-6P fibers (B), and the overgrown 6T/p-6P fibers (C).

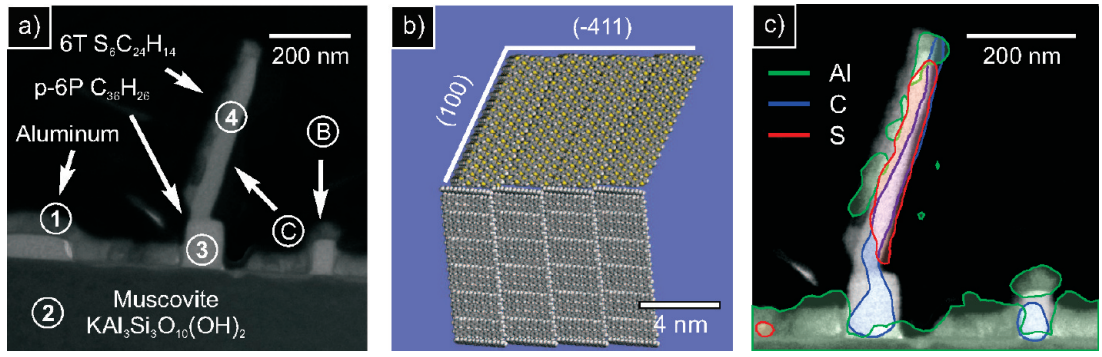

Figure 5. (a) TEM cross section of p-6P/6T heterostructure, indicating the deposited aluminum layer (1), muscovite mica substrate (2), p-6P template region (3), and 6T crystallite (4). (b) Simulated view along LFA of p-6P templates showing the expected angular alignment of 6T low energy (100) plane. (c) Scanning Auger investigation marking aluminum (green), carbon (blue), and sulfur (red) rich regions projected on top of the corresponding TEM image.

The magnification is taken from a 10 × 10 μm AFM image, and its origin is indicated by a white polygon in Figure 4b.

The AFM image in Figure 4b underlines further the high microscopic and macroscopic order of the fibers that can be up to several micrometers long and cover homogeneously the substrate surface. The corresponding height distribution is depicted in Figure 4c and reveals three characteristic height levels. Beside the sharpest peak (A, 10.5 nm) that can be clearly attributed to the bare substrate, two additional peaks are present. Further analysis of characteristic regions for the three height levels, marked in the AFM image of Figure 4b by white circles (A−C), shows the presence of two different fiber types. Comparing their mean height values obtained by AFM with the nominal layer thickness, the peak located at 122.6 nm (B) can be attributed to the bare p-6P fiber template, whereas the peak at 465.5 nm (C) can be correlated to the mean height of the overgrown p-6P/6T organic heterostructures characteristic for 90 min 6T deposition time. Strikingly, both structures do not only differ in height but also in shape, which becomes evident by AFM cross sections demonstrated in Figure 4c. Whereas fibers of type B are composed of nearly perfect rectangular shape, which is expected for p-6P crystallites,[22] the overgrown structures reveal a triangular rounded silhouette already hinting a different growth morphology.

For a detailed analysis of the cross-sectional shape of the heterostructures, transmission electron microscopy (TEM) has been applied, providing a nanoscopic view on the structural properties. Before preparing TEM slides, samples have been covered with a 25 nm thick aluminum (Al) layer for protection purposes, becoming visible by an inclosing cover layer, indicated in Figure 5a by region 1. Furthermore, the muscovite mica substrate can be clearly determined by a sharp contrast and is indicated by region 2. Structures characteristic for the two different fiber types are labeled B and C. In particular, rectangular appearance of fiber-type B in combination with a correlation in height justifies the direct comparison with AFM analysis. Strikingly, fiber structures of type C are characterized by a tilted entity on top of a rectangular fiber basement, emphasizing the difference in shape already observed by AFM analysis. In order to understand the observed behavior, molecular stacking has been modeled based on structural investigations determined by XRD pole figure measurements. The obtained result is indicated in Figure 5b, providing a cross-sectional view along the fiber directions and consequently comparable with TEM analysis. The lower part of the image indicates a single p-6P crystallite characterized by a horizontal alignment of its $\{11\bar{1}\}$ netplanes. On the contrary, $\{\bar{4}11\}$ netplanes of the overgrown 6T crystallite are aligned horizontally, fulfilling structural alignment deduced by XRD. The presented model stack directly reveals a different stacking of 6T and p-6P crystallites along the growth direction, which can be explained by the different tilt of low index planes, namely, $(001)_{p\text{-}6P}$ and $(100)_{6T}$, providing the lowest surface energy. Whereas p-6P low index plane is more or less oriented vertically, the low energy facet of 6T is remarkably tilted and astonishingly provides excellent agreement with experimental data (demonstrated in Figure 5a). In summary, this notable difference provides a clear picture of the organic−organic interface, which can be characterized by a well-defined epitaxial relationship between both organic crystallites. In order to overcome the weak phase contrast between 6T and p-6P crystallites obtained by TEM, mainly originating from the dominating carbon within the molecular structures, scanning Auger microscopy (SAM) investigations have been applied on the prepared TEM slide. In particular, it was scanned for aluminum, characteristic for the muscovite mica substrate and the protection layer, with carbon being present in p-6P as well as 6T and sulfur, providing a clear label for the presence of 6T molecules. The scan has been performed on the same sample position and is presented in Figure 5c, masking the corresponding TEM image by isointensity lines for aluminum (green), carbon (blue), and sulfur (red) rich regions. As expected, aluminum rich regions

can be found in the substrate and at the sample surface characteristic for the presence of the Al protection layer. Focusing on the organic fiber structures, carbon rich regions nicely coincide with the shape of both fiber cross sections and consequently give a detailed picture about the local distribution of p-6P or 6T molecules. In order to distinguish between both organic species, sulfur has been used as a unique fingerprint for the presence of 6T molecules. Strinkingly, red marked areas reveal the presence of 6T only in the upper and consequently tilted part of the fibers, emphasizing the deduced picture by TEM and XRD analysis. In particular, it can be stated that structural investigations result in a closed and consistent picture, proving the successful implementation of organic−organic heteroepitaxy on nanofiber templates.

CONCLUSION

In conclusion, we show by combining optical, structural, and morphology investigations that organic−organic heteroepitaxy can be used to produce multilayered organic nanofibers with high crystallinity, well-defined epitaxial relationship along different materials' phases, sharp molecular azimuthal order, and long-range morphological homogeneity. Directed growth of α-sexithiophene on a para-sexiphenyl fiber template on muscovite mica results in highly crystalline and oriented hetero-nanostructures with molecules laying parallel to the substrate, yielding strong optical polarization anisotropy in a broad band of wavelengths. Achievement of broad band optical waveguiding in blue, green, and red spectral regions could enlarge the horizon of potential applications of epitaxial organic nanofibers. Organic nanofibers featuring optical waveguiding and random lasing could enable the realization of active photonic sensors with high sensitivity.[11] Moving from single (blue) band operation of pure p-6P fibers to the triband operation based on heteroepitaxial p-6P/6T fibers would then allow for increasing sensing capabilities and data volumes.

METHODS

All samples have been fabricated on muscovite mica (001) substrates (SPI, Structure Probe, Inc.) by using hot wall epitaxy (HWE). Muscovite mica is a representative of sheet silicate minerals and provides a layered structure of aluminum silicate sheets weakly bound by layers of potassium ions. Each layer is characterized by a high symmetry direction identified by parallel aligned surface grooves. Between the individual sheets, the high symmetry direction alternates by 120°, leading to a periodic αβαβ stacking sequence along the (001) direction. Immediately after cleaving, the mica substrates were transferred *via* a load lock to the growth chamber, providing two separated HWE reactors equipped with p-6P (TCI) and 6T (Sigma-Aldrich) source material. The system is operated under high vacuum (HV) conditions with a nominal pressure of 9×10^{-6} mbar. The optimized evaporation temperature for p-6P (6T) is given at 240 °C (190 °C), leading to a nominal growth rate of 3 nm/min (4.5 nm/min). In order to avoid temperature gradients during growth and to reduce adsorbed species on the surface, the substrate has been preheated at 120 °C for 30 min. The chosen temperature is kept constant during the whole growth procedure. After depositing p-6P for 40 min (≅120 nm fiber height), the sample is automatically transferred in HV conditions to the 6T source oven. Subsequently, 6T has been deposited for 1 s up to 90 min (≅405 nm). It has to be stated that nominal layer thickness is defined as average fiber height within the presented article.

Epifluorescence images were acquired upon sample illumination by a Hg lamp spectrally narrowed in the 330−360 nm band or by a scanning GaN laser source emitting at 406 nm. For polarization-resolved fluorescence spectroscopy, organic structures are excited over a large area of some hundreds of square micrometers at 375 nm by a frequency-doubled Ti:sapphire oscillator with 82 MHz repetition frequency. Emission has been analyzed by a rotating linear polarizer, wavelength dispersed in a grating spectrometer, and detected by a liquid-nitrogen-cooled detector. Polarization-dependent spectra have been fitted by reference functions deduced from pure p-6P (blue), 6T (red) fiber structures grown on muscovite mica (Figure 2a). The emission spectrum of interface 6T submonolayer (green) is extracted from that of a p-6P/6T film grown on muscovite mica with short (<5 s) 6T exposure time upon weighted subtraction of the spectrum of pure p-6P fibers.

X-ray diffraction pole figure measurements were performed in Schultz reflective geometry using Cr Kα ($\lambda = 2.29$ Å) radiation. The used combination of the collimator size on the primary side and width of the slit optics at the secondary side together with the graphite monochromator results in an acceptance angle of ±0.5° around the fixed scattering angle 2Θ of the detector.

Atomic force microscopy (AFM) studies of the deposited nanofibers were performed using a Digital Instruments Dimension 3100 in the tapping mode. The AFM characterization was performed on an area of 10 μm^2 with a SiC tip. The pixel resolution was chosen with 512 × 512 pixels, which corresponds to 19.5 nm/pixel. The zero height has been corrected by leveling the data to the minimum height of the whole image.

Transmission electron microscopy (TEM) measurements were carried out on a JEOL 2011 microscope (200 kV, LaB6) attached with an OXFORD EDX-System for elemental analysis. Sample preparation with the focused ion beam technique was carried out using a ZEISS XB 1540 Crossbeam after depositing an aluminum protection layer by thermal evaporation.

The Auger images were taken at a tilt angle of 30° to the 30 kV primary electron beam and 30° to the concentric hemispherical analyzer (CHA) as a good compromise between distortion and count rate. The primary electron beam current was set to 10 nA, and the CHA operated in constant analyzer energy (CAE) mode with a pass energy of 500 eV to obtain maximum count rate at the expense of energy resolution of 10 eV. Each Auger image consists of 128 × 128 pixels with a dwell time of 50 ms per pixel. For the Al and the C image, the KLL Auger peaks at 1389 and 263 eV were used and for the S mapping of the LVV Auger peak at 146 eV, respectively.

Acknowledgment. This work has been financially supported by the Austrian Science Fund (FWF) Projects NFN-S9706 and NFN-S9708. Work in Cagliari was partially funded by MIUR through FIRB projects (Synergy-FIRBRBNE03S7XZ and FIRB-RBAU01N449) and by the European Commission through the Human Potential Programs (RTN Nanomatch, Contract No. MRTN-CT-2006-035884).

Supporting Information Available: Details about growth experiment and AFM analysis. Additional SEM and TEM images

are presented, including EDX spectra of representative sample positions. Original Auger images are also included, demonstrating how isointensity lines are deduced as presented in the article. This material is available free of charge *via* the Internet at http://pubs.acs.org.

REFERENCES AND NOTES

1. Mannsfeld, S. C. B.; Leo, K.; Fritz, T. Line-on-Line Coincidence: A New Type of Epitaxy Found in Organic−Organic Heterolayers. *Phys. Rev. Lett.* **2005**, *94*, 056104.
2. Timpanaro, S.; Sassella, A.; Borghesi, A.; Porzio, W.; Fontaine, P.; Goldmann, M. Crystal Structure of Epitaxial Quaterthiophene Thin Films Grown on Potassium Acid Phthalate. *Adv. Mater.* **2001**, *13*, 127–130.
3. Oehzelt, M.; Koller, G.; Ivanco, J.; Berkebile, S.; Haber, T.; Resel, R.; Netzer, F. P.; Ramsey, M. G. Organic Heteroepitaxy: *p*-Sexiphenyl on Uniaxially Oriented α-Sexithiophene. *Adv. Mater.* **2006**, *18*, 2466–2470.
4. Koller, G.; Berkebile, S.; Krenn, J. R.; Netzer, F. P.; Oehzelt, M.; Haber, T.; Resel, R.; Ramsey, M. G. Heteroepitaxy of Organic−Organic Nanostructures. *Nano Lett.* **2006**, *6*, 1207–1212.
5. Hernandez-Sosa, G.; Simbrunner, C.; Sitter, H. Growth and Optical Properties of α-Sexithiopene Doped Para-Sexiphenyl Nanofibers. *Appl. Phys. Lett.* **2009**, *95*, 013306.
6. Yanagi, H.; Morikawa, T. Self-Waveguided Blue Light Emission in p-Sexiphenyl Crystals Epitaxially Grown by Mask-Shadowing Vapor Deposition. *Appl. Phys. Lett.* **1999**, *75*, 187–189.
7. Andreev, A.; Matt, G.; Brabec, C.; Sitter, H.; Badt, D.; Seyringer, H.; Sariciftci, S. Highly Anisotropically Self-Assembled Structures of Para-Sexiphenyl Grown by Hot-Wall Epitaxy. *Adv. Mater.* **2000**, *12*, 629–633.
8. Balzer, F.; Rubahn, H.-G. Dipole-Assisted Self-Assembly of Light-Emitting p-nP Needles on Mica. *Appl. Phys. Lett.* **2001**, *79*, 3860–3862.
9. Yanagi, H.; Ohara, T.; Morikawa, T. Self-Waveguided Gain-Narrowing of Blue Light Emission from Epitaxially Oriented *p*-Sexiphenyl Crystals. *Adv. Mater.* **2001**, *13*, 1452–1455.
10. Balzer, F.; Bordo, V.; Simonsen, A.; Rubahn, H.-G. Optical Waveguiding in Individual Nanometer-Scale Organic Fibers. *Phys. Rev. B* **2003**, *67*, 115408.
11. Quochi, F. Random Lasers Based on Organic Epitaxial Nanofibers. *J. Opt.* **2010**, *12*, 024003and references therein.
12. Balzer, F.; Shamery, K. A.; Neuendorf, R.; Rubahn, H.-G. Nonlinear Optics of Hexaphenyl Nanofibers. *Chem. Phys. Lett.* **2003**, *368*, 307–312.
13. Kankate, L.; Balzer, F.; Niehus, H.; Rubahn, H.-G. Organic Nanofibers from Thiophene Oligomers. *Thin Solid Films* **2009**, *518*, 130–137.
14. Andreev, A.; Sitter, H.; Sariciftci, N. S.; Brabec, C. J.; Springholz, G.; Hinterdorfer, P.; Plank, H.; Resel, R.; Thierry, A.; Lotz, B. Highly Ordered Anisotropic Nano-Needles in Para-Sexiphenyl Films. *Thin Solid Films* **2002**, *403*, 444–448.
15. Sitter, H.; Andreev, A.; Matt, G.; Sariciftci, N. S. Hot Wall Expitaxial Growth of Highly Ordered Organic Epilayers. *Synth. Met.* **2003**, *138*, 9–13.
16. Becker, R. S.; de Melo, J. S.; Macuanita, A. L.; Elisei, F. Comprehensive Evaluation of the Absorption, Photophysical, Energy Transfer, Structural, and Theoretical Properties of α-Oligothiophenes with One to Seven Rings. *J. Phys. Chem.* **1996**, *100*, 18683–18695.
17. da Como, E.; Loi, M. A.; Murgia, M.; Zamboni, R.; Muccini, M. J-Aggregation in α-Sexithiophene Submonolayer Films on Silicon Dioxide. *J. Am. Chem. Soc.* **2006**, *128*, 4277–4281.
18. Baker, K. N.; Fratini, A. V.; Resch, T.; Knachel, H. C.; Adams, W. W.; Socci, E. P.; Farmer, B. L. Crystal Structures, Phase Transitions and Energy Calculations of Poly(*p*-phenylene) Oligomers. *Polymer* **1993**, *34*, 1571–1587.
19. Horowitz, G.; Backet, B.; Yassar, A.; Lang, P.; Demanze, F.; Fave, J. L.; Garnier, F. Growth and Characterization of Sexithiophene Single Crystals. *Chem. Mater.* **1995**, *7*, 1337–1341.
20. Resel, R.; Haber, T.; Lengyel, O.; Sitter, H.; Balzer, F.; Rubahn, H.-G. Origins for Epitaxial Order of Sexiphenyl Crystals on Muscovite (001). *Surf. Interface Anal.* **2009**, *41*, 764–770.
21. Jerome, B.; O'Brien, J.; Ouchi, Y.; Stanners, C.; Shen, Y. R. Bulk Reorientation Driven by Orientational Transition in a Liquid Crystal Monolayer. *Phys. Rev. Lett.* **1993**, *71*, 758–761.
22. Schiek, M.; Balzer, F.; Al-Shamery, K.; Brewer, J. R.; Lützen, A.; Rubahn, H.-G. Organic Molecular Nanotechnology. *Small* **2008**, *4*, 176–181.